Journal of Applied Electrochemistry **30**: 1109–1117, 2000.

Electrochemical synthesis of Cr(II) at carbon electrodes in acidic aqueous solutions

Q. YIN, N.P. BRANDON* and G.H. KELSALL
T.H. Huxley School of Environment, Earth Science and Engineering, Imperial College of Science, Technology and Medicine, London SW7 2BP, Great Britain
*(*author for correspondence, fax: +44 20 7594 7444, e-mail: n.brandon@ic.ac.uk)*

Received 18 January 2000; accepted in revised form 21 May 2000

Key words: carbon electrode, chromium (III)/(II), electrochemical synthesis, electrochemistry

Abstract

The electrochemical synthesis of Cr(II) has been investigated on a vitreous carbon rotating disc electrode and a graphite felt electrode using cyclic voltammetry, impedance spectroscopy and chronoamperometry. The results show that in 0.1 M Cr(III) + 0.5 M sulphuric acid and in 0.1 M Cr(III) + 1 M hydrochloric acid over an electrode potential range of −0.8 to 0.8 V vs SCE, the electrochemical reaction at carbon electrodes is essentially a surface process of proton adsorption and desorption, without significant hydrogen evolution and chromium(II) formation. At electrode potentials more negative than −0.8 V vs SCE, both hydrogen evolution and chromium(II) formation occurred simultaneously. At electrode potentials −0.8 to −1.2 V vs SCE, the electrochemical reduction of Cr(III) on carbon electrodes is controlled mainly by charge transfer rather than mass transport. Measurements on vitreous carbon and graphite felt electrodes in 1 M HCl, with and without 0.1 M $CrCl_3$, allowed the exchange current density and Tafel slope for hydrogen evolution, and for the reduction of Cr(III) to Cr(II), to be determined. The chromium(III) reduction on vitreous carbon and graphite electrodes can be predicted by the extended high field approximation of the Butler–Volmer equation, with a term reflecting the conversion rate of Cr(III) to Cr(II).

1. Introduction

As a strong reductant, chromium(II) has been studied for its application, *inter alia*, in organic synthesis [1–3], energy storage [4–7], and hydrometallurgy [8, 9]. In addition, Cr(III)/Cr(II) is typical of redox couples which involve one-electron outer-sphere or inner-sphere transfer, depending on the nature of the anions present in the electrolytes and electrode materials employed. Therefore, the electrochemical behaviour of the Cr(III)/Cr(II) redox couple has been investigated extensively in HCl [10, 11], $HClO_4$ [12, 13], $NaClO_4$, $Ca(ClO_4)_2$ [14, 15], and KPF_6 [16] electrolytes, together with basic aluminium chloride-1-methyl-3-ethylimidazolium chloride molten salts [17]. The electrode materials employed include hanging mercury drop [10, 14], dropping mercury [12, 15], mercury amalgam film [18], lead [19], titanium [11], platinum [16], silver [16, 18], gold [19], bismuth [20] and steel mesh [21]. The redox behaviour of chromium(III)/(II) coordinated with organic ligands, such as EDTA [20, 22] and ethylenediamine [23] has also been investigated.

To employ Cr(II) as a reductant in the synthesis of organic chemicals, or in energy storage or hydrometallurgy, the electrochemical synthesis of chromium(II) with a high current efficiency and acceptable specific electrical energy consumption is a prerequisite. However, the Nernst equation for the reaction:

$$Cr^{3+} + e^- \leftrightarrow Cr^{2+} \tag{1a}$$

$$E \text{ vs SCE/V} = -0.669 + 0.0592 \log((Cr^{3+})/(Cr^{2+})) \tag{1b}$$

indicates that the standard redox potential of Reaction 1 is more than 0.4 V lower than that of hydrogen evolution. To avoid this unwanted side reaction dominating the cathodic process, cathode materials for Cr(II) synthesis must have a small exchange current and/or a large Tafel slope for hydrogen evolution. Unfortunately, the three metals (Pb, Cd and Hg) with the highest hydrogen overpotentials, are also highly toxic, which could result in problems were corrosion to occur in a practical system.

Carbon electrodes have adequate electrical conductivity and chemical stability, together with fairly high hydrogen overpotentials [24, 25]. A number of authors have investigated the electrochemical behaviour of carbon electrodes, including vitreous carbon, carbon felt or cloth, and graphite felt or cloth [26–29] for the removal of heavy metals, such as copper, nickel, chromium, zinc, lead, mercury and uranium, and other hazardous materials from waste water and industrial effluents. A few correlations have been published to describe mass transfer processes at vitreous carbon or carbon felt electrodes [30–33]. However, no work on the

synthesis of Cr(II) on graphite felt electrodes has been reported.

The aim of this investigation was to study the electrochemical reduction of Cr(III) to Cr(II) on vitreous carbon and graphite felt electrodes, and to explore the feasibility of using graphite felt cathodes for the synthesis of Cr(II) in aqueous acidic solutions.

2. Experimental details

Analytical grade chromium(III) chloride, potassium chromium(III) sulphate, hydrochloric acid and sulphuric acid were used to prepare electrolytes without further purification. The water used was purified by reverse osmosis (Elga Elgastat) and deionization (Elga Prima) to give a resistivity of $1.6 \times 10^5\ \Omega$ m. The anolyte was 0.5 M H_2SO_4, the catholyte was chromium(III) chloride in hydrochloric acid, or potassium chromium(III) sulphate in sulphuric acid.

Most of the electrochemical experiments were carried out in a three-compartment cell with a Nafion® N324 or N417 cation permeable membrane to separate the catholyte and anolyte. Before each experiment, the electrolyte was purged with nitrogen for at least half an hour to desorb any dissolved oxygen. The nitrogen used was first itself deoxygenated by passing successively through (sodium) anthraquinone-2-sulfonate solution and chromium(II) solution, both prepared with zinc amalgam. The working electrode was either a vitreous carbon rotating disc electrode with an ash content of 0.04%, or a stationary graphite felt electrode with a thickness of 6 mm (Le Carbone Ltd, Brighton, UK). A saturated calomel electrode (SCE) was used as the reference electrode, assumed to have a potential of 0.245 V vs standard hydrogen electrode (SHE), and a platinum flag was used as the counter electrode. Some experiments were carried out in a flow-by reactor with a graphite felt cathode and anode, and operated in batch recycle mode. The current densities quoted in this work are all based on the apparent geometric area. All electrochemical experiments were performed with a computer controlled Princeton Applied Research 273A or Solartron 1286 potentiostat/galvanostat. A Hewlett Packard 8452A diode array spectrophotometer was used to monitor the aqueous chromium(III) absorption peak at a wavelength around 415 nm, enabling the catholyte composition, and hence current efficiencies, to be determined.

3. Results and discussion

Figure 1 shows the voltammograms obtained from a vitreous carbon electrode in 0.1 M $KCr(SO_4)_2 + 0.5$ M H_2SO_4, for which three reductive current peaks ((a), (b) and (c)) and two oxidative current peaks ((d) and (e)) are evident. In the 0.8 to −0.8 V vs SCE range, two reduction current peaks ((a) and (b)) were seen during the sweep from positive to negative potentials, but only one oxidation peak (d) was observed on the subsequent positive-going sweep. This suggests that the redox process corresponding to peak (b) is less reversible than that for peak (a). The magnitude of current peaks (a), (b) and (d) varied linearly with potential sweep rate, suggesting the process was one of surface electrochemical adsorption/desorption. The charge associated with the reduction peaks ((a) + (b)) and oxidation peak (d) were about 12 C m^{-2}, implying that a monolayer of vitreous carbon electrode surface was involved in these surface reactions, assuming one electron transfer process and a surface roughness factor of 3. In contrast, current peak c did not decrease linearly with sweep rate, and the associated charge increased significantly from 11.5 to 87 C m^{-2} as the sweep rate decreased from 200 to 10 mV s^{-1}. In addition, no corresponding oxidation peak occurred in the cyclic voltammograms when the potential was swept back in the positive-going direction, suggesting that reduction products were dispersed into the bulk electrolyte.

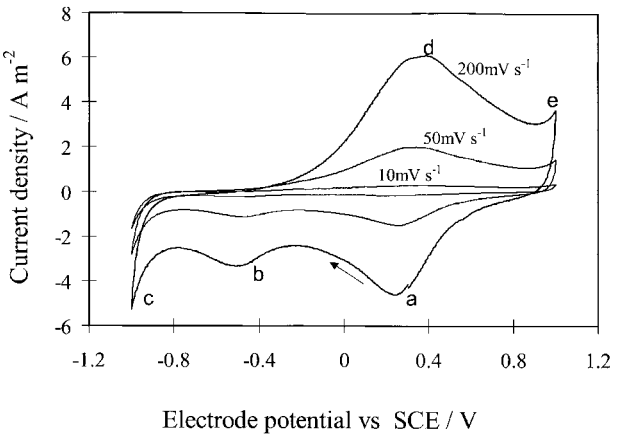

Fig. 1. Cyclic voltammograms of a vitreous carbon electrode in 0.1 M $KCr(SO_4)_2$ + 0.5 M H_2SO_4 at sweep rates of 10, 50 and 200 mV s^{-1}.

From thermodynamic considerations and the preliminary analysis above, the five current peaks (a) to (e) have been tentatively assigned to the following reactions:

$$\text{peak (a) and (b): } -C_xO_y(\text{surf.}) + z\text{H}^+ + z\text{e}^- \rightarrow -C_xO_yH_z(\text{surf.}) \quad (x > y \geq 0) \tag{2}$$

$$\text{peak (c): } Cr^{3+} + e^- \rightarrow Cr^{2+} \tag{3}$$

$$2\,\text{H}^+ + 2\,\text{e}^- \rightarrow \text{H}_2 \tag{4}$$

$$\text{peak (d): } -C_xO_yH_z(\text{surf.}) - z\text{e}^- \rightarrow -C_xO_y(\text{surf.}) + z\text{H}^+ \quad (x > y \geq 0) \tag{5}$$

$$\text{peak (e): } 2\,H_2O \rightarrow O_2 + 4\,\text{H}^+ + 4\,\text{e}^- \tag{6}$$

In Equations 2 and 5, the species C_xO_y stands for the Bronsted basic sites at the vitreous carbon electrode surface. When $y > 0$, it represents the functional groups such as quinonoid and lactone [34–36]. When $y = 0$, it represents the surface carbon atoms with dangling bonds, on which protons may be adsorbed at a negative electrode potential.

This assignment is supported by comparison of the cyclic voltammograms obtained in 0.5 M H_2SO_4, with and without chromium ions (Figure 2). The figure shows that when the electrolyte of 0.1 M $KCr(SO_4)_2$ + 0.5 M H_2SO_4 was replaced by one containing only 0.5 M H_2SO_4, reduction current peaks (a), (b) and oxidation current peak (d) were almost unchanged, whereas reduction current peak (c) became smaller. This indicates that in the potential region −0.8 to 0.8 V vs SCE, the redox current arises mainly from the electrochemical adsorption/desorption of protons, while chromium ions are essentially not involved in the process. Only when the electrode potential was more negative than −0.8 V vs SCE did the reduction of Cr(III) become evident. The voltammograms in Figure 3 indicate that the magnitude of the current peaks (a), (b), (c) and (d) were pH dependent, giving further support to the assignment above.

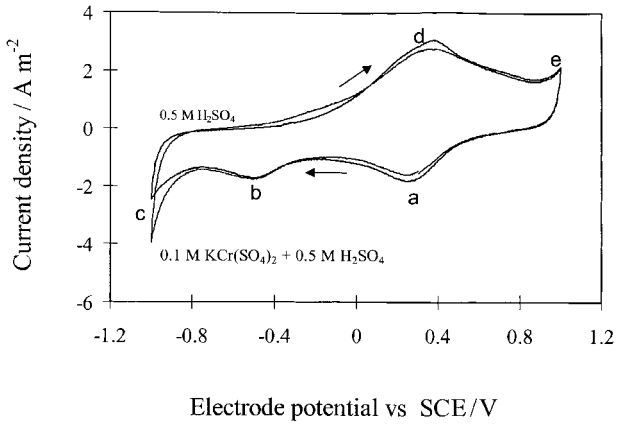

Fig. 2. Comparison of the cyclic voltammograms at a vitreous carbon electrode in 0.1 M $KCr(SO_4)_2$ + 0.5 M H_2SO_4 and 0.5 M H_2SO_4 at a sweep rate of 100 mV s^{-1}.

The impact of mass transfer on peak (c), attributed to either Cr(III) reduction or H_2 evolution, is further depicted in Figure 4, which shows cyclic voltammograms of a vitreous carbon electrode at a sweep rate of 20 mV s^{-1} in 0.1 M $KCr(SO_4)_2$ + 0.5 M H_2SO_4, with rotation rates of 4 and 49 Hz. No current plateau was evident in the voltammograms, and the current densities were essentially independent of rotation rate, indicating that the reduction process was not mass transport controlled. For a rotating disc electrode, the mass transport limit current density can be predicted by the Levich equation:

$$j_L = 1.554\, nFD^{2/3}v^{-1/6}f^{1/2}c \tag{7}$$

where n is the number of electrons transferred per mole of reactant, F is Faraday's constant, c is the bulk concentration of Cr(III) with diffusion coefficient D, v is the kinematic viscosity of the electrolyte and f is the electrode rotation rate (Hz). Using values of $v \approx 1.2 \times 10^{-6}$ m^2 s^{-1} and $D \approx 5.9 \times 10^{-10}$ m^2 s^{-1} for Cr(III) in aqueous solutions [15, 37], the relationship between the limiting current density j_L and rotation rate can be determined.

Combining the Levich equation with the Butler–Volmer equation at high overpotential, the relationship between the Cr(III) reduction current density, electrode potential and rotation rate can be expressed by the equation:

$$j = \left[j_0 j_L \exp\left(-\frac{\alpha nF\eta}{RT}\right)\right] \times \left[j_L + j_0 \exp\left(-\frac{\alpha nF\eta}{RT}\right)\right]^{-1} \tag{8}$$

From Equations 7 and 8 and the exchange current determined in the following sections, the relationship between electrode potential, rotation rate and current

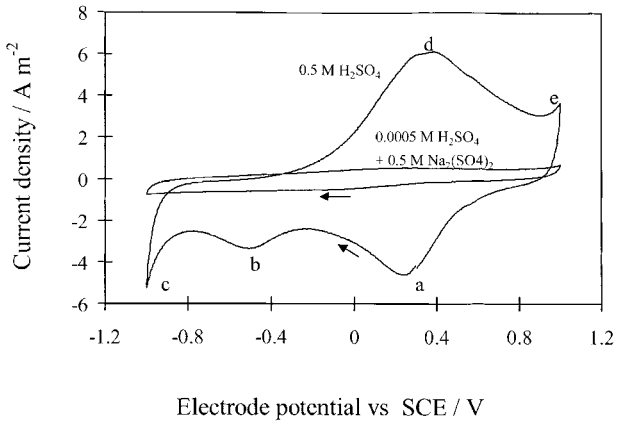

Fig. 3. Comparison of the cyclic voltammograms at a vitreous carbon electrode in 0.0005 M H_2SO_4 + 0.5 M $Na_2(SO_4)_2$, and 0.5 M H_2SO_4 at a sweep rate of 200 mV s^{-1}.

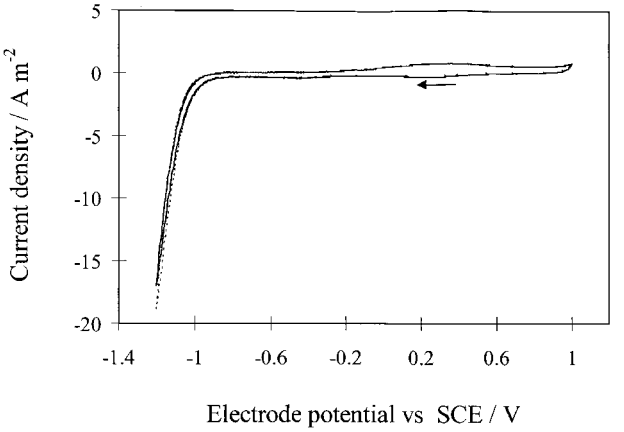

Fig. 4. Cyclic voltammograms of a vitreous carbon electrode in 0.1 M $KCr(SO_4)_2$ + 0.5 M H_2SO_4 at a sweep rate of 20 mV s^{-1} and rotation rates of (——) 4 and (– – –) 49 Hz.

density for a vitreous carbon electrode in 0.1 M $KCr(SO_4)_2$ + 0.5 M H_2SO_4 can be determined, and is illustrated in Figure 5. It shows that the cathodic limiting current is predicted to be achieved only at electrode potentials <-1.4 V vs SCE, whereas the standard redox potential for the reduction of Cr^{2+} to Cr metal is -1.15 V vs SCE. The predicted limiting cathodic currents are equal to approximately 200 and 1000 A m^{-2} for rotation rates of 4 and 49 Hz, respectively, much larger than the measured currents shown in Figure 4. It can also be seen from Figure 5 that at -1.2 V vs SCE, rotation rate has little effect on the reduction current density. All of these indicate that the Cr^{3+} reduction process is essentially controlled by charge transfer, consistent with the experimental results shown in Figure 4.

Figure 6 shows the effect of extending the negative potential limit on the redox processes of Cr(III)/Cr(II) at a vitreous carbon electrode in 0.1 M $KCr(SO_4)_2$ + 0.5 M H_2SO_4; little effect was evident until the potential limit was <-1 V vs SCE. For greater clarity, the current density at the different negative potential limits and the sum of reductive and oxidative charge in one cycle, were determined, as shown in Figure 7. It indicates that the reduction current densities were all less than 1 A m^{-2} at negative electrode potential limits of 0.0 V, -0.4 V and -0.8 V vs SCE, suggesting that the vitreous carbon electrode had a relatively small exchange current density and a high overpotential for the reduction of protons and chromium(III). Therefore, to obtain a reasonable reduction current density, the electrode potential should be controlled in a potential range more negative than -0.8 V vs SCE.

The possible cause for the slow electrochemical reduction of protons may be the relatively stable and strong bonding between oxygen-hydrogen and/or carbon-hydrogen. This means that once O—H and/or C—H bonding takes place at the electrode surface in the early stage of reduction process, as described by Reaction 2, it needs a higher cathodic activation energy to break the bonds and release molecular H_2. The slow reduction of Cr(III) to Cr(II) may be interpreted by the Frank–Condon principle. In 0.1 M $KCr(SO_4)_2$ + 0.5 M H_2SO_4, the electron and ligand configuration of $Cr(H_2O)_6^{3+}$ significantly differs from $Cr(H_2O)_6^{2+}$. For complex $Cr(H_2O)_6^{3+}$, the three d-electrons of Cr(III) are evenly filled in the t_{2g} orbitals with equivalent energy, resulting in a complex with an octahedral structure which is stable and substitution inert. In contrast, the four d-electrons of Cr(II) in complex $Cr(H_2O)_6^{2+}$ are located in split t_{2g} and e_g orbitals with different energy levels, causing severe Jahn–Teller distortions away from the normal octahedral structure, and making ligand substitution labile. When Cr(III) is reduced to Cr(II), one electron in the t_{2g} orbitals has to overcome the separation energy barrier and be excited into e_g orbitals. These substantial changes in electron and ligand configuration during the reduction of Cr(III) to Cr(II) may retard the charge transfer rate significantly.

From the total charge passed in one cycle (Figure 7), it can be seen that as the negative electrode potential limit was extended from 0.0 to -0.8 V vs SCE, the

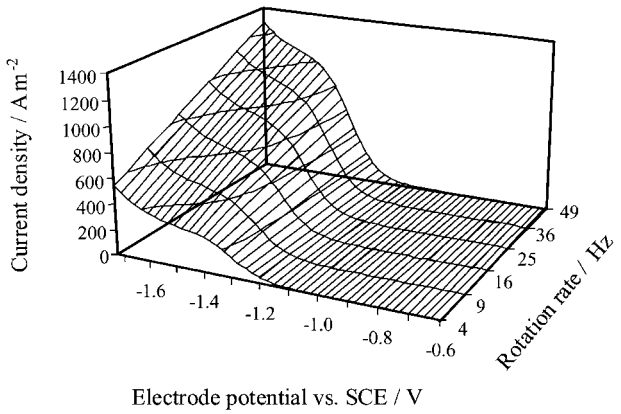

Fig. 5. Predicted relationship between electrode potential, rotation rate and current density for a vitreous carbon electrode in 0.1 M $KCr(SO_4)_2$ + 0.5 M H_2SO_4.

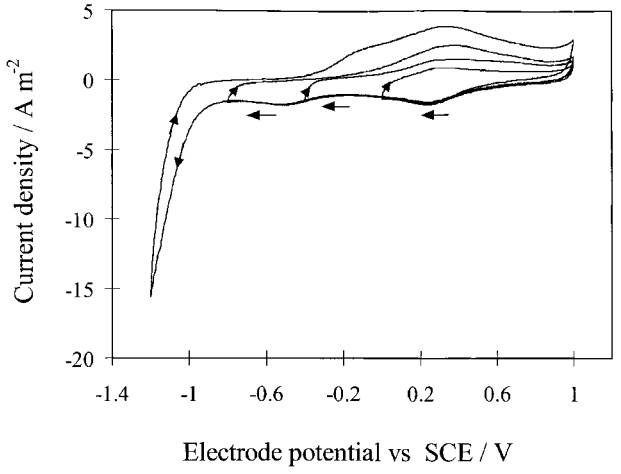

Fig. 6. Cyclic voltammograms at a vitreous carbon electrode in 0.1 M $KCr(SO_4)_2$ + 0.5 M H_2SO_4 at a sweep rate of 100 mV s^{-1} with varied negative potential limits.

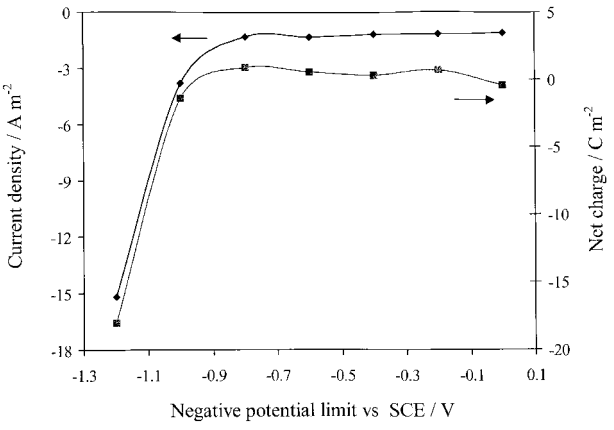

Fig. 7. Relationships between negative potential limit, current density and net charge passed in one cycle for a vitreous carbon electrode in 0.1 M $KCr(SO_4)_2$ + 0.5 M H_2SO_4 at a sweep rate of 100 mV s^{-1}.

reductive and oxidative charge in one cycle was approximately equal, such that the total net charge varied around zero. This suggests that when the electrode potential was swept in the negative direction, reduction products were adsorbed at the electrode surface. As the electrode potential was swept back from the negative potential limit in the positive-going direction, the adsorbed reduction products were reoxidized, such that the whole process was essentially one of surface electrochemical adsorption/desorption, as described by Reactions 2 and 5. When the negative electrode potential limit extended to lower than −1 V vs SCE, the total negative charge passed in one cycle increased significantly, indicating that the reduction Reactions 3 and 4 started to dominate the cathodic process, forming Cr(II) and H_2, which then dispersed from the electrode surface into the bulk solution.

Figure 8 shows the voltammograms obtained from a vitreous carbon electrode in 0.1 M $CrCl_3$ + 1 M HCl, which exhibited characteristics very similar to those obtained in 0.1 M $KCr(SO_4)_2$ + 0.5 M H_2SO_4 (Figure 1). For example, there are five current peaks ((a) to (e)) in the voltammograms; peaks (a), (b) and (d) varying linearly with potential sweep rate, and the charges associated with the reduction peaks ((a) + (b)) and oxidation peak (d) were about 12 C m^{-2}. However, the reduction current (peak (c)) of Cr(III) to Cr(II) in 0.1 M $CrCl_3$ + 1 M HCl was significantly greater than that in 0.1 M $KCr(SO_4)_2$ + 0.5 M H_2SO_4. This may be attributed to the effect of the pathway difference in electron transfer between electrode and Cr(III) ions on the reaction rate. It is well established that the reduction of complex $Cr(H_2O)_6^{3+}$ is via an outer-sphere pathway, whereas the reduction of $Cr(H_2O)_5Cl^+$ or $Cr(H_2O)_4Cl_2^+$ is via an inner-sphere pathway [13, 16]. With the latter mechanism, the chloride ions are able to penetrate the outer Helmholtz plane and attach to the electrode surface, acting as a bridge between the electrode and Cr(III) ions to enhance electron transfer.

Figure 9 shows two Tafel plots of the vitreous carbon electrode in 1 M HCl, with and without $CrCl_3$. Neglecting any interaction effects (e.g., due to adsorbed hydrogen blocking sites for Cr(III) reduction) then subtraction of plot (a) (obtained in 1 M HCl) from plot (b) (obtained in 1 M HCl + 0.1 M $CrCl_3$) should represent the current density of Cr(III) reduction. From this data, the exchange current density and Tafel slope for hydrogen evolution in 0.1 M Cr(III) + 1 M HCl were determined to be 5.86×10^{-4} A m^{-2} and 0.27 V $decade^{-1}$; whereas for the reduction of Cr(III) to Cr(II) they were 1.58×10^{-3} A m^{-2} and 0.12 V $decade^{-1}$, respectively. The exchange current density for the reduction of Cr(III) to Cr(II) is only a little greater than that for hydrogen evolution, but the Tafel slope for the reduction of Cr(III) to Cr(II) is much smaller than that for hydrogen evolution. This means that, under optimised conditions, chromium(II) can be synthesized on a vitreous carbon electrode with a high current efficiency.

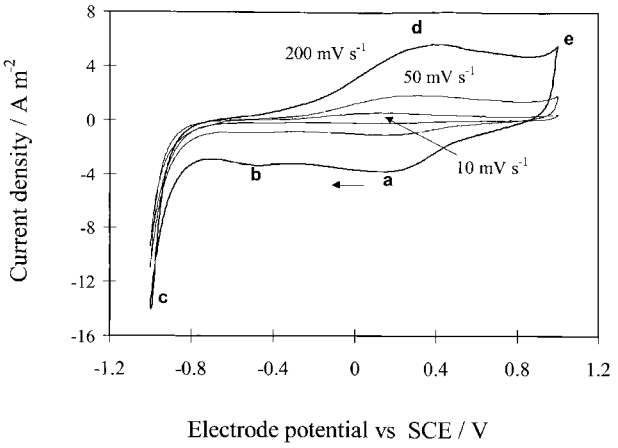

Fig. 8. Cyclic voltammograms at a vitreous carbon electrode in 0.1 M $CrCl_3$ + 1 M HCl at sweep rates of 10, 50 and 200 mV s^{-1}.

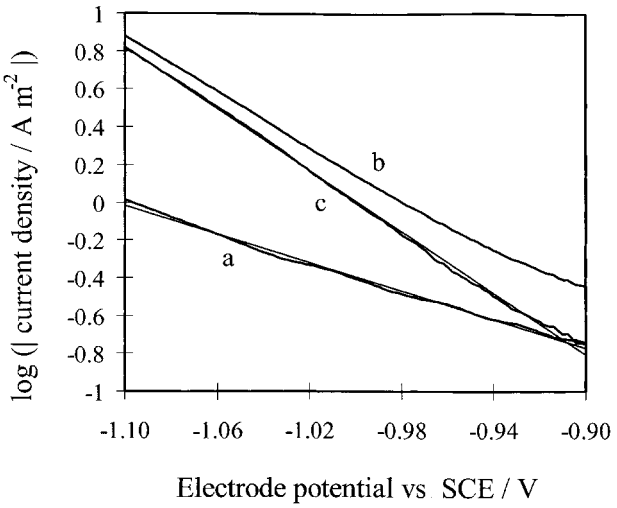

Fig. 9. Quasi-steady current density against electrode potential of a rotating vitreous carbon disc electrode at a rotation rate of 16 Hz and a sweep rate of 1 mV s^{-1} in (a) 1 M HCl, (b) 1 M HCl + 0.1 M $CrCl_3$ and (c) curve (a) subtracted from curve (b).

On the basis of these results, the hydrogen evolution kinetics can be predicted by the high field approximation of the Butler–Volmer equation:

$$j_{H_2} = -j_{0,H_2} \exp(-2.303\,\eta/b_{H_2}) \tag{9}$$

whereas chromium(III) reduction may be predicted by the extended high field approximation of the Butler–Volmer equation incorporating a term involving the mass transport controlled current density (j_L) to allow for local depletion of Cr(III):

$$j_{Cr(III)} = -j_{0,Cr(III)} \exp(-2.303\eta/b_{Cr(III)})/[1-(j_{0,Cr(III)}/j_L) \times \exp(-2.303\eta/b_{Cr(III)})] \tag{10}$$

Moreover, potentiostatic reduction of Cr(III) in a constant volume isothermal batch reactor with a constant total dissolved chromium concentration Cr_T (Cr_T = Cr(III) + Cr(II)), will result in conversion(X)-dependent

overpotentials and exchange current densities, the latter parameter being given by

$$j_{0,\mathrm{Cr(III)}} = Fk_0([\mathrm{Cr}_{(\mathrm{III})}]^{\alpha}[\mathrm{Cr}_{(\mathrm{II})}]^{(1-\alpha)}) = Fk_0([\mathrm{Cr_T}](1-X))^{\alpha}([\mathrm{Cr_T}]X)^{(1-\alpha)} \quad (11)$$

From Equations 9 to 11, the relationship between the electrode potential, Cr(III) concentration and current efficiency may be predicted, as illustrated by Figure 10, assuming a mean mass transport rate coefficient $k_m = 2 \times 10^{-5}\,\mathrm{m\,s^{-1}}$ and transfer coefficient $\alpha = 0.5$. Since the total concentration Cr_T in the electrolyte is 0.1 M and constant, the Cr(III) concentration is therefore an indicator of the conversion of Cr(III) to Cr(II). Figure 10 shows that the current efficiency decreases on increasing the conversion of Cr(III) to Cr(II). When the electrode potential is controlled in the range from -0.9 to -1.2 V vs SCE, the current efficiency is predicted to reach more than 0.9 at current densities in the range from 0.4 to 30 A m^{-2}. When the electrode potential is lower than -0.9 V vs SCE or higher than -1.2 V vs SCE, the current efficiency will be significantly decreased. However, this analysis neglects: (i) interactions between the Cr(III) and proton reduction processes, assuming them to be simply additive, (ii) possible formation of chromium metal at potentials $< E^{\circ}(Cr^{2+}/Cr) = -1.15$ V vs SCE and the resulting catalysis of hydrogen evolution, (iii) the effect of oxygen diffusion into catholyte, causing an effective loss in current efficiency for Cr(II) formation.

As with vitreous carbon, graphite felt also has adequate electrical conductivity coupled with excellent chemical resistance; moreover, it has greater specific surface area and lower cost. The electrochemical properties of graphite felt are similar to that of vitreous carbon in general, but there was an evident difference in their voltammograms, as will be discussed below. Figure 11 shows the cyclic voltammograms of a graphite

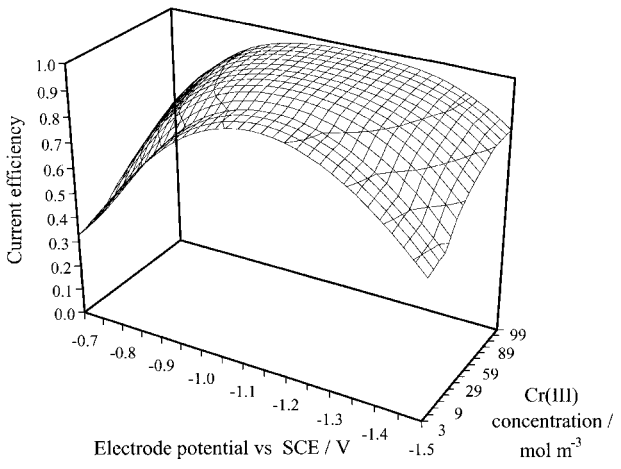

Fig. 10. Predicted relationship between electrode potential, current efficiency and concentration of Cr(III) in 1 M HCl + 0.1 M (Cr(III) + Cr(II)) at a vitreous carbon electrode.

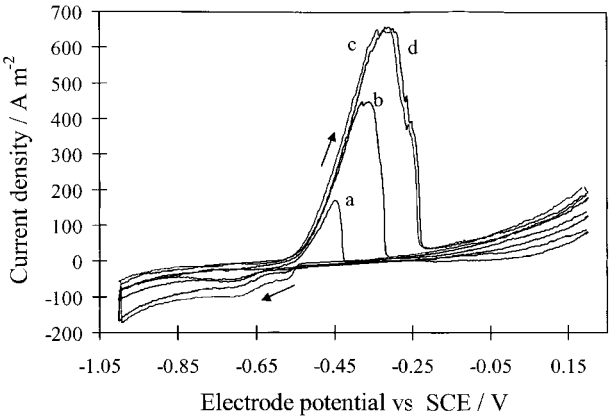

Fig. 11. Cyclic voltammograms for a graphite felt electrode with sweep rate of 20 mV s^{-1} in 1 M HCl + 0.1 M $CrCl_3$, and held at a negative potential limit of -1 V vs SCE for (a) 160 s, (b) 1×10^3 s, (c) 5×10^3 s, (d) 1×10^4 s before sweeping the potential back to positive values.

felt electrode with a sweep rate of 20 mV s^{-1} in 1 M HCl + 0.1 M $CrCl_3$. The voltammograms (a), (b), (c) and (d) were obtained when the electrode potential was swept to -1 V vs SCE, then held at that potential for 160 s, 1000 s, 5000 s and 10000 s, respectively, before the electrode potential was swept back to positive values.

It can be seen that the longer the electrode was held at negative potential limit -1 V vs SCE in 1 M HCl + 0.1 M $CrCl_3$, the greater was the oxidation current peak on the subsequent positive-going sweep. However, this oxidation peak disappeared as the electrode potential was reversed from the positive electrode potential limit. Moreover, if the electrolyte 1 M HCl + 0.1 M $CrCl_3$ was replaced by 1 M HCl, the oxidation peak did not occur in either the negative-going or positive-going potential sweep. Therefore, the oxidation current peak may be attributed to the accumulation and subsequent oxidation of Cr(II) ions formed at the graphite felt electrode when the electrode potential was swept in the negative-going direction and held at the negative potential limit. The accumulation of Cr(II) product within graphite felt electrode would be enhanced by two factors compared to the vitreous carbon electrode. First, the porosity within the graphite felt electrode encourages a build-up of the Cr(II) product, which is liable to be oxidised back to Cr(III) on the positive-going potential sweep. Secondly, the crystal structure of graphite consists of hexagonal rings stacked in layers. Within the layer, the carbon–carbon atoms through sp^2 hybridization form a strong sigma-bond with a length of 0.142 nm, whereas between the layer, carbon–carbon atoms form weaker π-bond with a length of 0.335 nm. On the other hand, the ionic radii of Cr(III) and Cr(II) in crystalline form are 0.063 nm and 0.089 nm respectively [37]. According to the Debye–Huckel theory and the Poisson–Boltzmann equation, the radii of the ionic cloud of Cr(III) and Cr(II) in 0.1 M $CrCl_3$ + 1 M HCl electrolyte would be approximately

0.13 and 0.18 nm, respectively. This suggests that Cr(III) and Cr(II) ions in the aqueous electrolyte may find it difficult to enter the vitreous carbon lattice, but are likely to intercalate graphite layers through the edge plane of graphite felt. This process may be expressed by the reaction:

$$C + xCr(III) + xe^- \leftrightarrow C\cdots xCr(II) \quad (12)$$

From the voltammograms (a), (b), (c) and (d) in Figure 11, the oxidation charge densities associated with the current peak in the potential range from −0.25 to −0.55 V vs SCE were 520, 2790, 5850 and 5860 C m^{-2}, respectively, corresponding to 5.4×10^{-3}, 2.9×10^{-2}, 6.7×10^{-2} and 6.7×10^{-2} mol m^{-2} of Cr(II) ions adsorbed and intercalated within the graphite felt electrode. The voltammograms show peaks (c) and (d) are almost superimposed, and the amount of charge corresponding to current peaks (c) and (d) were equal with each other, suggesting that the Cr(II) adsorption and/or intercalation approached saturation (i.e., 6.7×10^{-2} mol m^{-2}) when the holding time was $\geqslant$5000 s at a potential of −1 V vs SCE.

Figure 12 shows the quasi-steady Tafel plots of the graphite felt electrode in 1 M HCl with 0.1 M $CrCl_3$ (plot (b)) and without $CrCl_3$ (plot (a)). Plot (c) in the Figure was obtained by subtraction of curve (a) from curve (b). After linear regression of this data, the apparent exchange current density and apparent Tafel slope on a graphite felt electrode in 1 M HCl and 0.1 M Cr(III) + 1 M HCl were determined to be 1.86×10^{-2} A m^{-2} and 0.32 V $decade^{-1}$ for hydrogen evolution, and 5.19×10^{-2} A m^{-2} and 0.145 V $decade^{-1}$ for chromium(III) reduction. On the basis of the experimental results and Equations 9 to 11, neglecting potential distribution in the graphite felt, the relationship between the electrode potential, current efficiency and concentration of Cr(III) can be predicted and illustrated in Figure 13. It indicates that the optimum electrode potential is in the region from −0.9 to −1.2 V vs SCE. At the beginning of the synthesis, the current efficiency can be higher than 0.9 and then gradually decreases to approximately 0.8 as more and more Cr(III) is converted to Cr(II).

To synthesize Cr(II) and validate the theoretical prediction, a recycle electrochemical flow-by reactor with a graphite felt working electrode of apparent geometric area 30 cm^2 was designed and constructed. Chromium(II) synthesis was carried out at different electrode potentials using chronoamperometry techniques. From the decay of the adsorbance peak of Cr(III) at approximately 415 nm, the conversion of Cr(III) to Cr(II) was determined and monitored by an UV–visible spectrophotometer as a function of elapsed time (Figure 14). The current efficiency obtained experimentally and theoretically predicted as a function of electrode potential are plotted in Figure 15, showing that the current efficiency could reach about 0.85 at a conversion of Cr(III) to Cr(II) of 0.8, and in the current density range of about 20 to 100 A m^{-2}, in agreement with the theoretical prediction. These values would be

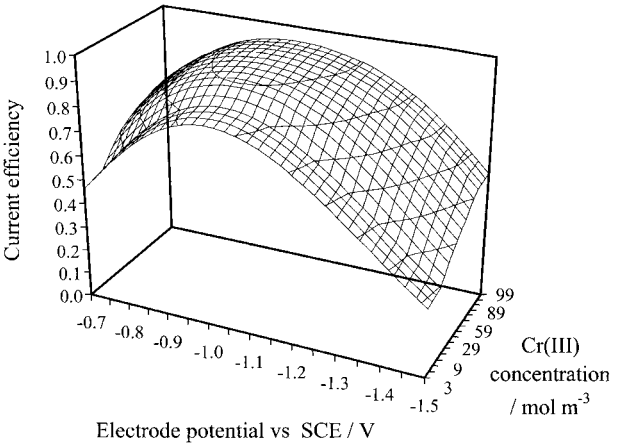

Fig. 13. Predicted relationship between graphite felt electrode potential, current efficiency and concentration of Cr(III) in 1 M HCl + 0.1 M (Cr(III) + Cr(II)) at a graphite felt electrode.

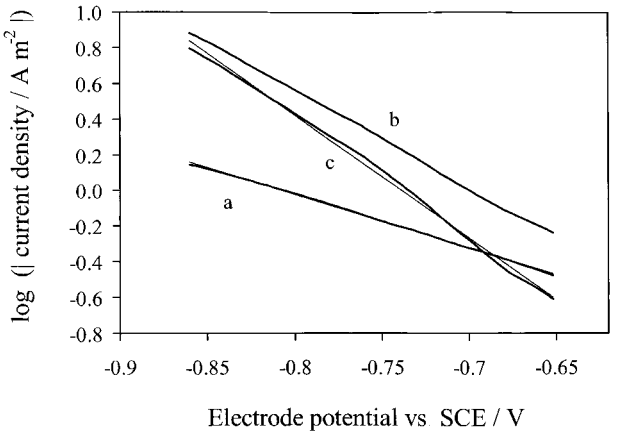

Fig. 12. Quasi-steady current density vs electrode potential of a carbon felt electrode at a rotation rate of 16 Hz and a sweep rate of 1 mV s^{-1} in (a) 1 M HCl, (b) 1 M HCl + 0.1 M $CrCl_3$ and (c) curve (a) subtracted from curve (b).

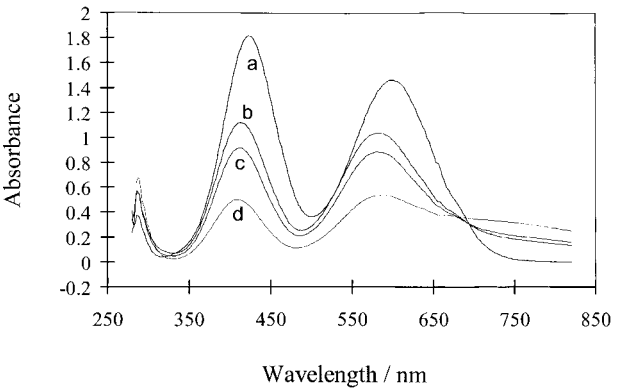

Fig. 14. UV–visible spectra for 0.1 M Cr(III) in 1 M HCl before and after reduction at −1.2 V vs SCE for different times and passed charge. (a) before reduction, (b) 1.52 hours and 1.71 kC, (c) 2.34 h and 2.38 kC, (d) 3.87 h and 3.56 kC.

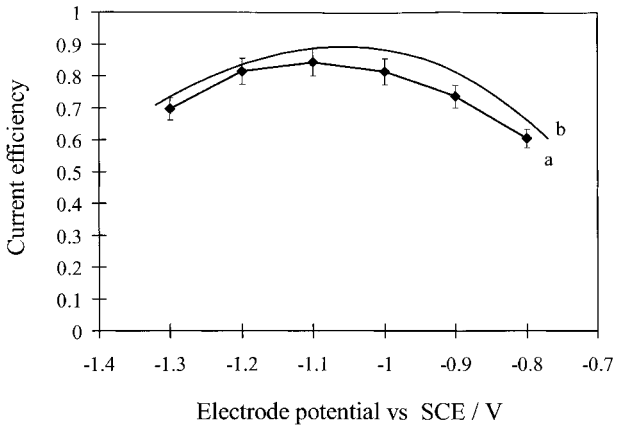

Fig. 15. Relationship between current efficiency and graphite felt electrode potential for the reduction of Cr(III) to Cr(II) at a conversion of 0.8 in 0.1 M $CrCl_3$ + 1 M HCl, (a) experimental measurement and (b) theoretical prediction.

higher for higher concentration of Cr(III); for example, a current efficiency of 0.98 are predicted at a conversion of 0.8 from an initial concentration of 1 kmol Cr(III) m^{-3}. The reasonable agreement between experimental and theoretically predicted current efficiency, in spite of neglecting the 3D nature of the graphite cathode, is probably due to the slow kinetics and high Tafel slopes causing penetration of the current into the felt in spite of the reaction not being transport controlled.

4. Conclusions

In 0.1 M Cr(III) + 0.5 M sulphuric acid and 0.1 M Cr(III) + 1 M hydrochloric acid over an electrode potential range from −0.8 to 0.8 V vs SCE, the electrochemical reaction at carbon electrodes was essentially a surface process of proton adsorption and desorption, without significant hydrogen evolution and chromium(II) formation. At electrode potentials more negative than −0.8 V vs SCE, both hydrogen evolution and chromium(II) formation occurred simultaneously. The electrochemical reduction of Cr(III) on vitreous carbon electrodes was mainly controlled by charge transfer rather than mass transfer.

Graphite felt electrodes showed similar electrochemical properties to vitreous carbon electrodes, but Cr(III) and Cr(II) ions are more liable to intercalate into the graphite layers than the vitreous carbon lattice. The chromium(III) reduction kinetics can be predicted by the extended high field approximation of the Butler–Volmer equation. In the prediction, a term involving the mass transport and the conversion rate of Cr(III) to Cr(II) was incorporated to allow for local depletion of Cr(III) concentration. Both theoretical predictions and experimental results show that when the electrode potential was controlled at around −1.1 V vs SCE with a fractional conversion of 0.8, the current efficiency for Cr(III) reduction to Cr(II) could reach about 0.85 for an initial concentration of 0.1 kmol Cr(III) m^{-3}.

Acknowledgement

The authors thank the UK Engineering and Physical Sciences Research Council for a grant providing a research fellowship for Q. Yin.

References

1. W. Traube and W. Lange, *Ber. Deutsch. Chem. Ges.* **58** (1925) 2773.
2. F.A. Anet and E. Isabelle, *Can. J. Chem.* **36** (1958) 589.
3. C.E. Castro, *J. Am. Chem. Soc.* **83** (1961) 1601.
4. L.H. Thaller, Dept. of Energy, DC, DOE/NaSa1002-79/3, Washington, DC, NASA TM-79143 (1979).
5. Moonlight Project: 'Advanced Battery Electric Energy Storage System', NEDO, 10, Japan (1988).
6. M.A. Climent, P. Garces, M. Lopez-Segura and A. Aldaz, *An. Quim.* **83** (1987) 12.
7. M. Lopez-Atalaya, G. Codina, J.R. Perez, J.L. Vazquez, A. Aldaz and M.A. Climent, *J. Power Sources* **35** (1991) 225.
8. C.I. House and G.H. Kelsall, *in* 'Extractive Metallurgy 85', IMM, London (1985), p. 659.
9. W.L. Staker, *US Patent 543 208* (1975).
10. G.H. Kelsall, C.I. House and F.P. Gudyanga, *J. Electroanal. Chem.* **244** (1988) 179.
11. T. Hirato and Y. Awakura, *in* 4th International Symposium on Electrochemistry in Mineral and Metal Processing, Los Angeles, CA (May 1996), Electrochemical Society, NJ, p. 368.
12. R. Andreu and F. Sanchez, *J. Electroanal. Chem.* **210** (1986) 111.
13. M.J. Weaver and F.C. Anson, *Inorg. Chem.* **15** (1976) 1871.
14. M. Zielinska-Ignaciuk and Z. Galus, *J. Electroanal. Chem.* **50** (1974) 41.
15. R. Andreu, M. Rueda, D. Gonzalez-Arjona and F. Sanchez, *J. Electroanal. Chem.* **175** (1984) 251.
16. S.W. Barr, K.L. Guyer and M.J. Weaver, *J. Electroanal. Chem.* **111** (1980) 41.
17. J.S.Y. Liu, P.Y. Chen, I.W. Sun and C.L. Hussey, *J. Electrochem. Soc.* **144** (1997) 2388.
18. L.M. Yudi, A.M.B. Aruzzi and V.M. Solis, *J. Appl. Electrochem.* **18** (1988) 417.
19. H.Y. Liu, J.T. Hupp and M.J. Weaver, *J. Electroanal. Chem.* **179** (1984) 219.
20. C.D. Wu, D.A. Scherson, E.J. Calvo, E.B. Yeager and M.A. Reid, *J. Electrochem. Soc.* **133** (1986) 2109.
21. D. Pletcher and J.C.P. White, *Electrochim. Acta* **37** (1992) 575.
22. R. Meier, *J. Electroanal. Chem.* **263** (1989) 175.
23. M.J. Weaver and T.L. Satterberg, *J. Phys. Chem.* **81** (1977) 1772.
24. M.B. Redmount and E.A. Heintz, The manufacture of graphite electrodes, *in* H. Marsh, E.A. Heintz and F.R. Reinoso (eds), 'Introduction to Carbon Technologies' (Universidad de Alicante, Secretariado de Publicaciones, 1997).
25. M.R. Tarasevicch and E.I. Khrushcheva, Electrocatalytic properties of carbon materials, *in* B.E. Conway, J.O.M. Bockris and R.E. White (eds), 'Modern Aspects of Electrochemistry', Vol. 19 (1989).
26. I.C. Agarwal, A.M. Rochon, H.D. Gesser and A.B. Sparling, *Water Res.* **18** (1984) 232.
27. D. Golub and Y. Oren, *J. Appl. Electrochem.* **19** (1989) 311.
28. B. Delanghe, S. Tellier and M. Astruc, *Environ. Technol.* **11** (1990) 999.
29. F.C. Walsh, D. Pletcher, I. Whyte and J.P. Millington, *J. Chem. Tech. Biotechnol.* **55** (1992) 147.
30. N. Vatistas, P.F. Marconi and M. Bartolozzi, *Electrochim. Acta* **36** (1991) 339.

31. D. Pletcher, I. Whyte, F.C. Walsh and J.P. Millington, *J. Appl. Electrochem.* **21** (1991) 659.
32. R. Carta, S. Palmas, A.M. Polcaro and G. Tola, *J. Appl. Electrochem.* **21** (1991) 793.
33. K. Kinoshita and S.C. Leach, *J. Electrochem. Soc.* **129** (1982) 1993.
34. H.P. Boehm, *Adv. Catal.* **16** (1966) 179.
35. V.A. Garten, D.E. Weiss and J.B. Willis, *Aust. J. Chem.* **10** (1957) 295.
36. J.B. Donnet, *Carbon* **20** (1982) 267.
37. D.R. Lide (Ed.), 'CRC Handbook of Chemistry and Physics', 80th edn, (London/New York, 1999–2000).